Journal of Bionic Engineering (2023) 20:612–627
https://doi.org/10.1007/s42235-022-00280-3

RESEARCH ARTICLE

sEMG-Based Lower Limb Motion Prediction Using CNN-LSTM with Improved PCA Optimization Algorithm

Meng Zhu[1] · Xiaorong Guan[1] · Zhong Li[1] · Long He[1] · Zheng Wang[1] · Keshu Cai[2]

Received: 28 June 2022 / Revised: 25 September 2022 / Accepted: 27 September 2022 / Published online: 31 October 2022

Abstract

In recent years, sEMG (surface electromyography) signals have been increasingly used to operate wearable devices. The development of mechanical lower limbs or exoskeletons controlled by the nervous system requires greater accuracy in recognizing lower limb activity. There is less research on devices to assist the human body in uphill movements. However, developing controllers that can accurately predict and control human upward movements in real-time requires the employment of appropriate signal pre-processing methods and prediction algorithms. For this purpose, this paper investigates the effects of various sEMG pre-processing methods and algorithms on the prediction results. This investigation involved ten subjects (five males and five females) with normal knee joints. The relevant data of the subjects were collected on a constructed ramp. To obtain feature values that reflect the gait characteristics, an improved PCA algorithm based on the kernel method is proposed for dimensionality reduction to remove redundant information. Then, a new model (CNN + LSTM) was proposed to predict the knee joint angle. Multiple approaches were utilized to validate the superiority of the improved PCA method and CNN-LSTM model. The feasibility of the method was verified by analyzing the gait prediction results of different subjects. Overall, the prediction time of the method was 25 ms, and the prediction error was 1.34 ± 0.25 deg. By comparing with traditional machine learning methods such as BP (backpropagation) neural network, RF (random forest), and SVR (support vector machine), the improved PCA algorithm processed data performed the best in terms of convergence time and prediction accuracy in CNN-LSTM model. The experimental results demonstrate that the proposed method (improved PCA + CNN-LSTM) effectively recognizes lower limb activity from sEMG signals. For the same data input, the EMG signal processed using the improved PCA method performed better in terms of prediction results. This is the first step toward myoelectric control of aided exoskeleton robots using discrete decoding. The study results will lead to the future development of neuro-controlled mechanical exoskeletons that will allow troops or disabled individuals to engage in a greater variety of activities.

Keywords CNN · LSTM · Exoskeleton · sEMG · Knee trajectory · PCA · Bionic robot

✉ Xiaorong Guan
gxr@njust.edu.cn

Meng Zhu
zhumeng0120@njust.edu.cn

Zhong Li
zhong0814@njust.edu.cn

Long He
helong208@126.com

Zheng Wang
wangzheng19@njust.edu.cn

Keshu Cai
caikeshu@sina.com

[1] School of Mechanical Engineering, Nanjing University of Science and Technology, No. 200, Xiaolingwei, Nanjing City, Jiangsu Province, China

[2] Department of Rehabilitation Medicine, The First Affiliated Hospital of Nanjing Medical University, 300 Guangzhou Road, Nanjing City, Jiangsu Province, China

1 Introduction

Over the past few decades, there has been growing research interest in assistive exoskeletal robots. An exoskeleton is a wearable device used to enhance the physical function of an injured or disabled person during daily activities. Exoskeletons can be used in many applications, such as assisting workers or soldiers in reducing the weight they bear while performing tasks and helping patients perform repetitive rehabilitation training [1–6]. However, fewer studies have been conducted on gadgets that aid the human body in doing uphill movements. Huang, R. et al., [7] proposed an adaptive gait planning method with dynamic motion primitives for a lower limb exoskeleton to assist the human body in uphill motion. The experimental results showed that the proposed gait planning method made the human exoskeleton system more stable in uphill scenarios. Seo, K. et al., [8] developed a hip exoskeleton to enhance gait function in the elderly and rehabilitation of post-stroke patients. In practice, human–machine communication has been crucial to ensuring the performance and comfort of the exoskeleton system as a whole [9]. Various data recording systems, such as accelerometers, gyroscopes, and barometers, have become available due to developments in wearable sensor technology [10]. Various data-recording technologies, such as accelerometers, gyroscopes, and barometers, are now available due to improvements in wearable sensor technology. However, the wearer's movement intent hinders the development of this technology, as standard exoskeleton sensors cannot forecast movement tendencies. Existing research [11] has shown that surface EMG signals can provide information about neuromuscular activity and be used to control exoskeletons. EMG signals are biological signals used to measure the electrical activity of skeletal muscles. EMG signals can reflect muscular contraction force 30–100 ms earlier than other wearable sensors [12]. Intramuscular EMG (invasive) and surface EMG (non-invasive) are the two methods for recording EMG signals [13]. Comparatively, the noninvasive approach permits electrodes without physician supervision, discomfort, or infection risk [14]. Currently, SEMG signals are widely used in various applications such as upper [15] and lower extremity [16] exoskeletal control, neuromuscular disease examination [17], health and exercise monitoring [18].

Numerous researchers have investigated machine learning and deep learning models for identifying limb activities for controlling exoskeletons or prostheses. Chen, Y. et al., [19] proposed a low-cost Soft Exoskeleton Glove (SExoG) system for bilateral training that is powered by sEMG signals from a non-paralyzed hand. The experiments demonstrated that the hybrid model could achieve an average accuracy of 98.7% with four hand motions. Cisnal A. et al., [20] created a thresholded non-pattern recognition EMG-driven controller that detects gestures from a healthy hand and repeats them on an exoskeleton worn by a paralyzed hand. The study's findings revealed a 97 percent overall accuracy for gesture detection and indicated that the system was adequately time-responsive.

The surface EMG signal of the lower extremities is more intricate than that of the upper extremities. Lower extremity muscles are deeply buried beneath the skin and significantly overlap, making a prediction of motion based on surface EMG data from the lower extremity more complicated than that of the upper extremities. Zhuang, Y. et al., [21] suggested an EMG-based Conductance Control Strategy (ECCS). The system incorporates an EMG-Driven Musculoskeletal Model (EDMM), a conductance filter, and an internal position controller. ECCS is excellent at enhancing motor stability and has the potential to be utilized in robot-assisted rehabilitation to treat foot drops. Lyu, M. X. et al., [22] have designed an EMG-controlled knee exoskeleton to aid in the rehabilitation of stroke patients. The EMG signal of the patient was captured via an easy-to-wear EMG sensor and then processed by a Kalman filter to drive the exoskeleton autonomously. The test results demonstrated that individuals could use their EMG signals to control the exoskeleton.

High-quality signals provide more information needed for intention prediction, thus improving the prediction accuracy. However, different interventions and interferences are inevitable during the collection of sEMG signals [10]. Changes in patch position, sweat on the surface of the human skin, and EMG sensor transmission issues can affect data gathering during trials. Numerous signal processing applications, particularly in the communication and medical areas, require the pre-processing of sensor data to decrease noise. It becomes challenging to minimize the effects of signal interference. In reality, numerous researchers have researched ways to reduce signal noise pollution. Hajian, G. et al., [23] proposed a method for channel selection utilizing Fast Orthogonal Search (FOS) to increase estimation power. The method uses PCA in the frequency domain to identify the channel that contributes the most to the first principal component. The results demonstrate that the proposed method may minimize the dimensionality of the data (the number of channels is reduced from 21 to 9) while increasing the estimating power's precision. Combining nonlinear time series analysis and time–frequency domain approaches, Wang, G. et al., [24] proposed a wavelet-based correlation dimensionality method for extracting the effective features of sEMG signals. Results indicate four separate clusters corresponding to different forearm motions at the third resolution level, with a classification accuracy of one hundred percent when using two channels of SEMG signals. This indicates that the proposed method is suitable for classifying different

forearm motions. Sapsanis, C. et al., [25] proposed a pattern recognition method for identifying basic hand movements using sEMG data. Their experiments used Empirical Mode Decomposition (EMD) to decompose the EMG signal into an eigenmode function, followed by a feature extraction stage. The outcomes demonstrate that the application of EMD can enhance the recognition of traditional feature sets generated from the original EMG signal.

Deep learning techniques have developed rapidly in recent years. Compared with machine learning, deep learning focuses more on learning sample data's intrinsic patterns and representation levels. The information obtained from these learning processes can considerably assist when interpreting text, visuals, and sounds. CNN is a type of feedforward neural network that incorporates convolutional computation and has a deep structure; they are also one of the representative algorithms of deep learning. By their hierarchical structure, CNN is capable of representational learning and classifying incoming data in a manner that is translation-invariant. CNN has also demonstrated effectiveness in identifying time-series data such as EEG [26], EMG [27], and ECG [28] signals. LSTM is a temporal recurrent neural network that can process data by learning the data dependencies based on time-sequential data, making it suited for processing and forecasting events with time intervals and delays [29].

Inspired by the constraints of CNN and the benefits of LSTM, this study proposes a hybrid CNN-LSTM model. The model combines feature extraction and time series regression for deep learning to use the Spatio-temporal correlation of surface EMG signals fully. By extracting the deep features of CNN and performing LSTM processing, it is possible to predict complex EMG signals accurately. Moreover, the proposed prediction model is more precise and effective. In addition, an improved PCA based on the kernel approach is proposed for processing experimentally acquired sEMG data to solve the classic PCA's constraints in addressing the issue of nonlinear data. The remaining sections are organized as follows. Section 1 discusses the experiments and methods in detail, including experimental design, data collection, and data preprocessing. Sections 2 and 3 describe the pre-processing data methods and prediction models used in this paper. Section 4 compares the experimental results in different cases (including different dimensions and different methods). Section 5 discusses the results of the calculations. Finally, Sect. 6 concludes the paper.

2 Materials and Methods

2.1 Data Acquisition

2.1.1 Acquisition of sEMG Signal

sEMG is a technique used in research to examine the creation, recording, and interpretation of EMG signals. When physiological changes occur in the state of muscle fiber membranes, sEMG signals are created. Delsys is a global leader in designing, producing, and marketing high-performance EMG equipment (sales@delsys.com). Since its inception in 1993 in Natick, Massachusetts, Delsys has been focused on addressing the engineering issues involved with wearing EMG sensors. These challenges include low signal artifacts, low crosstalk, signal reliability, and signal consistency. This experiment uses the TrignoTM wireless EMG (a wireless surface EMG acquisition device from Delsys, USA) to acquire EMG signals. This device has a sensing delay of less than 500us and is equipped with 16 sensors with a maximum sampling rate of 4000 Hz. To prevent signal loss, a sampling rate of 2000 Hz was adopted for the trials. In this experiment, the TrignoTM system can simultaneously activate the Codamotion (3D motion capture) system, ensuring that the EMG data correlates to the knee joint angle data when data analysis is performed. Due to the symmetry of the human body during motion, data from only one leg (the right leg) were collected and analyzed for this experiment. According to the recommendations [30], 16 muscles on the right leg were selected as signal acquisition points. Figure 1 illustrates the location of the sensor paste. Prior to the experiment, selected locations were cleaned with medical alcohol to guarantee that EMG signals could be effectively acquired. It is essential to note that the sensors must be firmly attached to the muscles to prevent the EMG signal collector from deflecting during the activity. The distance between every two sensors is approximately 30 mm to reduce crosstalk. Otherwise, data loss may occur.

2.1.2 Acquisition of Joint Angle

In this experiment, Codamotion's 3D motion capture technology was used to collect human knee joint angle data. Codamotion is a provider of motion capture devices for academic research, healthcare applications and other life science markets (info@codamotion.com). The device consists of two cameras (to capture the trajectory of the marker points), a computer (to solve and store the data), and several marker points. The sampling rate of the device was adjusted to 200 Hz. Each Codamotion marker point was uniquely coded according to the Rizzoli [31] protocol specifications. As depicted in Fig. 2, three markers (1, 2, and 3) were

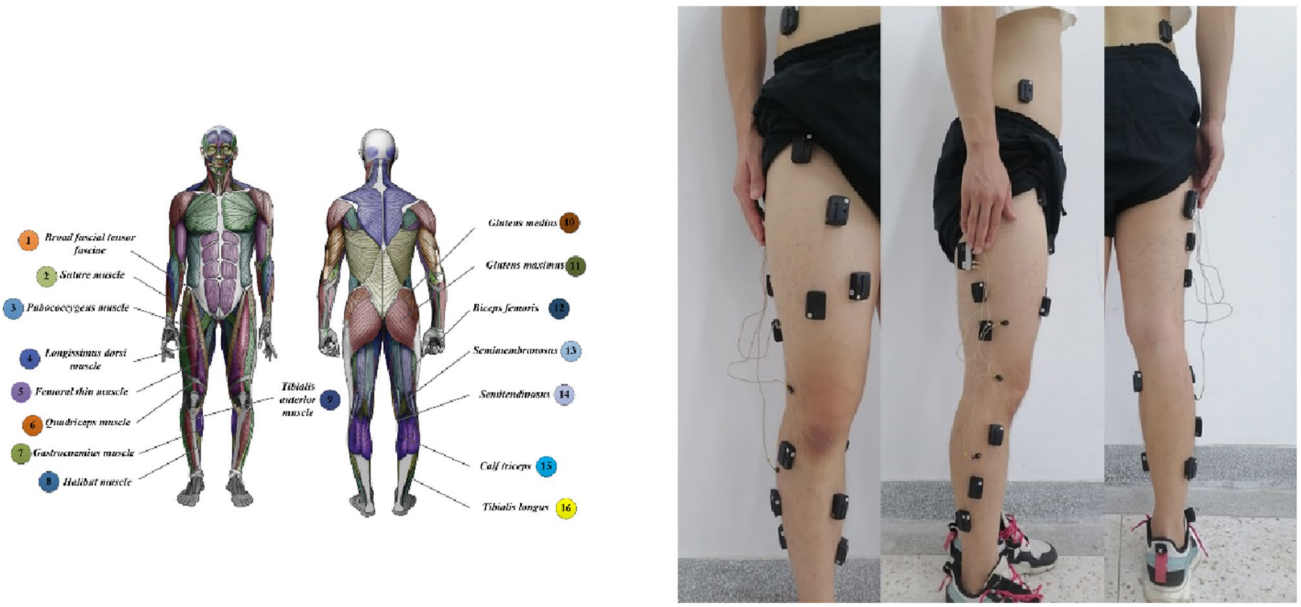

Fig. 1 Location of sensor attachment

Fig. 2 Location of the sensor attachment

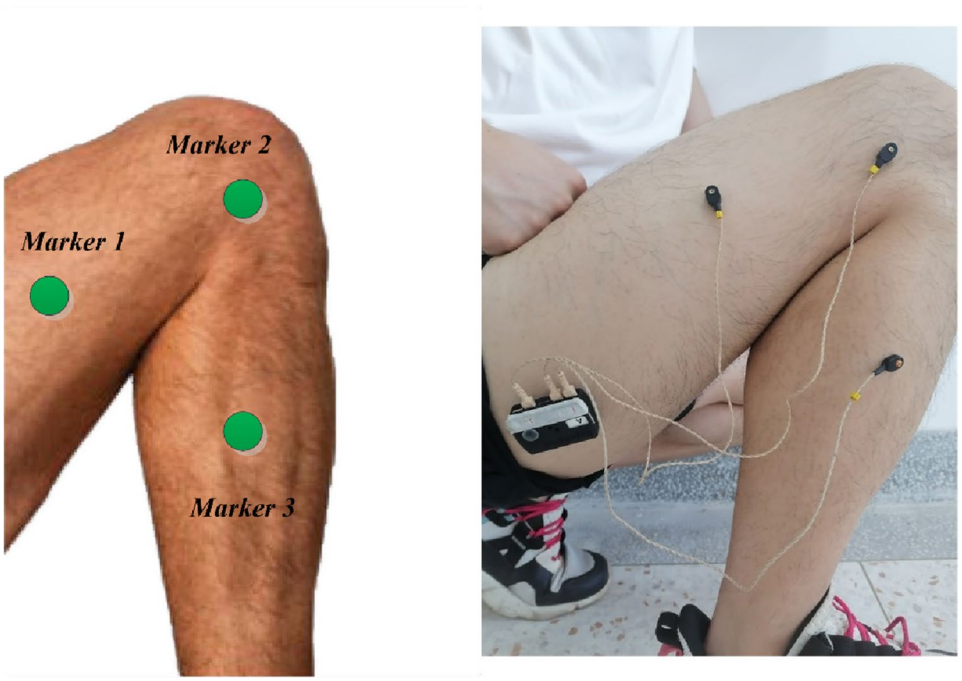

applied to the subject's knee joint. At the start of each trial, the EMG system activates the Codamotion system and collects the marker points' spatial coordinate coordinates in real-time. The markers transmit their acquired data to the host computer through the data collection box.

2.2 Experimental Procedures

Ten volunteers (five males and five females) participated in this experiment. The subjects did not suffer from leg sprain and had no painful muscle discomfort. Their ages ranged from 22 to 26 years, with a mean age of 24.2(±1.13) years, a height of 171.8(±7.23) cm, and a weight of 66.6(±9.29) kg. All volunteers were informed and signed a consent form before participating in the experiment. Table 1 provides

Table 1 Basic information of the volunteers

	Weight (Kg)	Height (cm)	Age (years)	Gender
Sub1	85	186	25	Male
Sub2	70	173	24	Male
Sub3	72	176	24	Male
Sub4	65	168	22	Male
Sub5	77	180	24	Male
Sub6	62	170	23	Female
Sub7	60	165	26	Female
Sub8	55	162	25	Female
Sub9	59	171	25	Female
Sub10	61	167	24	Female

Fig. 3 Experimental site

information about the volunteers who participated in the experiment.

The experiment was approved by the Review Committee of the First Hospital of Nanjing Medical University and conducted in accordance with the Declaration of Helsinki. The ethical review number for this experiment is 2021-SR-109. We designed and built the device to simulate the uphill condition, as shown in Fig. 3. The uphill angle of the device was set at 30 deg. Each set of the experiment lasted 20 s. During this period, participants were asked to perform uphill activities according to the frequency of the metronome (at a speed of 3KM/h). As suggested [30], all volunteers were instructed to conduct 3–5 min of low-intensity exercise prior to the trial. During the experiment, the sEMG signal of the volunteers will be simultaneously captured with the knee motion coordinate data. The experiment was repeated 80 times for the same volunteer. To reduce data fluctuations due to muscle fatigue, subjects will be asked to rest for 3 min for every five experiments performed.

2.3 Signal Pre-processing

The sEMG signal is a weak electrical signal, which is the result of the integrated superposition of action potential sequences emitted from many motor units on the skin surface. During the signal recording process, the sEMG signal is susceptible to interference from other electromagnetic signals [32]. Therefore, the SEMG signal must be preprocessed before utilizing the model prediction. Butterworth filters [33] and Chebyshev filters [34] are the most often used digital filters. According to [14], most of the EMG signal's

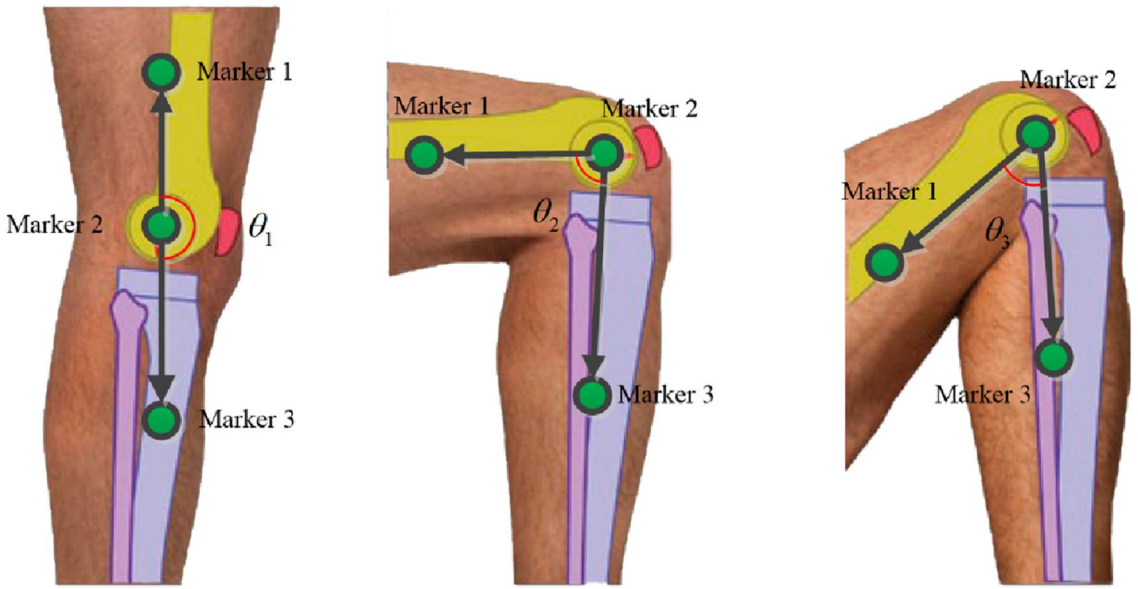

Fig. 4 The diagram for solving angles of motion

frequencies lie between 10 and 500 Hz. Consequently, this paper utilizes a fourth-order Butterworth bandpass filter to filter the sEMG signal.

It is worth mentioning that the coordinates acquired in the experiment cannot be employed directly. These coordinates were solved as a continuously variable angle to facilitate model prediction. The link vector model was utilized to solve this problem. Two neighboring points ($1 \rightarrow 2$, $2 \rightarrow 3$) are linked as vectors, and spatial coordinates of the three markers are employed (as shown in Fig. 4). Then, the angle between the two vectors may be computed using Codamotion's built-in solver. In this method, the coordinates recorded by the experiment are translated into a continuously changing angle.

The formula for the angle calculation is shown below.

$$\theta = \arccos \frac{\vec{m}.\vec{n}}{|\vec{m}|.|\vec{n}|}. \tag{1}$$

Since the sampling rates of the SEMG signal and the knee angle signal are different, the nearest neighbor interpolation method is used after the signal filtering is completed. The knee angle signal corresponds to the processed SEMG signal. In this way, 10*80 = 800 independent sets of data were obtained. We picked the EMG and knee angle data corresponding to the beginning of the exercise from the relevant data sets to generate a new set according to the subject number. The new dataset has 17 dimensions; x_1–x_{16} were EMG data, and y were knee angles. The data were standardized in accordance with recommendations [35] to shorten the learning time of the model and increase the accuracy of the predictions. The processed sMEG and knee angles are illustrated in Fig. 5.

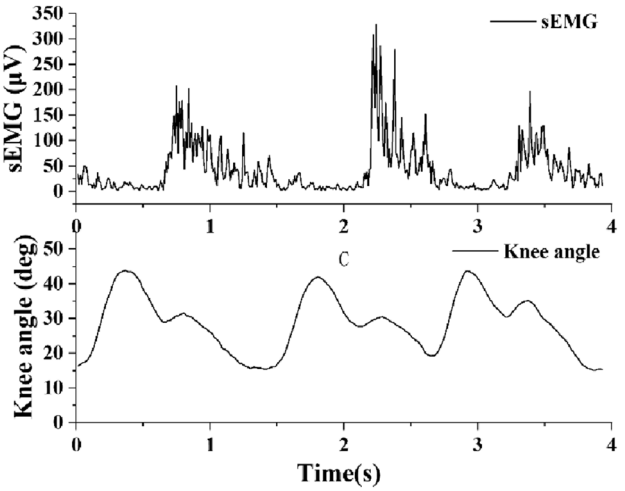

Fig. 5 Data visualization of sEMG and joint angle

3 Data Preprocessing Algorithms

3.1 Traditional PCA Algorithm

PCA (Principal Component Analysis) is one of the most widely used data dimensionality reduction algorithms. The main idea of PCA is to map n-dimensional features to k-dimensions, which are new orthogonal features also called principal components and are reconstructed from the original n-dimensional features. The work of PCA is to sequentially find a set of mutually orthogonal axes from the original space. The selection of new axes is closely related to the data itself. The first new axis is chosen to be the direction with the largest variance in the original data, the second new axis is chosen to be the plane orthogonal to the first axis that makes the largest variance, and the third axis is the plane orthogonal to the first and second axes that make the largest variance. By analogy, n such axes can be obtained. The procedure of PCA calculation is shown as follows.

First, the projections of the all pixels x_j onto this normalized direction v are $V^T x_1, \ldots V^T x_N$

The variance of the projections is

$$\begin{aligned} \sigma^2 &= \frac{1}{N}\sum_{i=1}^{N}\left(V^T - 0\right)^2 = \frac{1}{N}\sum_{i=1}^{N}\left(V^T x_i\right)\left(V^T x_i\right) \\ &= \frac{1}{N}\sum_{i=1}^{N} V^T x_i x_i^T v = v^T\left(\frac{1}{N}\sum_{i=1}^{N} x_i x_i^T\right)v = v^T C v, \end{aligned} \tag{2}$$

where:

$$C = \frac{1}{N}\sum_{i=1}^{N} x_i x_i^T. \tag{3}$$

Then the first principal vector can be found by the following equation:

$$v = \underset{v \in R^d, v=1}{argmax} v^T C v. \tag{4}$$

This is equivalent to finding the largest Eigenvalue of the following eigenvalue problem:

$$\begin{cases} Cv = \lambda v \\ \|v\| = 1 \end{cases}. \tag{5}$$

Note that:

$$C = \frac{1}{N}\sum\nolimits_{i=1}^{N} x_i x_i^T = \frac{1}{N}\left[x_{1,\ldots} x_N\right]\begin{bmatrix} x_1^T \\ \vdots \\ x_N^T \end{bmatrix}. \tag{6}$$

If:

$$X^T = [x_1, \ldots x_N]. \tag{7}$$

Then:

$$C = \frac{1}{N} X^T X. \tag{8}$$

Note that XX can be translated to:

$$C = \frac{1}{N}\sum_{i=1}^{N} \varphi(x_1)\varphi(x_i)^T = \frac{1}{N}[\varphi(x_1), \ldots \varphi(x_N)] \begin{bmatrix} \varphi(x_1)^T \\ \vdots \\ \varphi(x_N)^T \end{bmatrix}. \tag{9}$$

If:

$$X^T = [\varphi(x_1), \ldots \varphi(x_N)]. \tag{10}$$

Then:

$$C = \frac{1}{N} X^T X. \tag{11}$$

3.2 Improved PCA Algorithm

Note that the kernel matrix can be computed by kernel function K:

$$\begin{aligned} K = XX^T &= \begin{bmatrix} \varphi(x_1)^T \\ \vdots \\ \varphi(x_N)^T \end{bmatrix} [\varphi(x_1), \ldots \varphi(x_N)] \\ &= \begin{bmatrix} \varphi(x_1)^T\varphi(x_1) & \cdots & \varphi(x_1)^T\varphi(x_N) \\ \vdots & \ddots & \vdots \\ \varphi(x_N)^T\varphi(x_1) & \cdots & \varphi(x_N)^T\varphi(x_N) \end{bmatrix} \\ &= \begin{bmatrix} \kappa(x_1, x_1) & \cdots & \kappa(x_1, x_N) \\ \vdots & \ddots & \vdots \\ \kappa(x_N, x_1) & \cdots & \kappa(x_N, x_N) \end{bmatrix}. \end{aligned} \tag{12}$$

Then we can use K to find the eigenvectors of X^TX.

The eigenvalue problem of $K = XX^T$ is:

$$(XX^T)u = \lambda u \tag{13}$$

$$X^T(XX^T)u = \lambda X^T u \Rightarrow (X^TX)(X^Tu) = \lambda(X^Tu). \tag{14}$$

This means that X^Tu is an eigenvector of X^TX.

The eigenvalue v of X^TX can be computed by the eigenvalue of $K = XX^T$:

$$v = \frac{1}{X^Tu} X^T u = \frac{1}{\sqrt{u^T XX^T u}} X^T u = \frac{1}{\sqrt{u^T(\lambda u)}} X^T u = \frac{1}{\sqrt{\lambda}} X^T u, \tag{15}$$

where λ is the corresponding eigenvalue of u.

Finally, the projection of the testing sample $\varphi(x')$ can be computed by

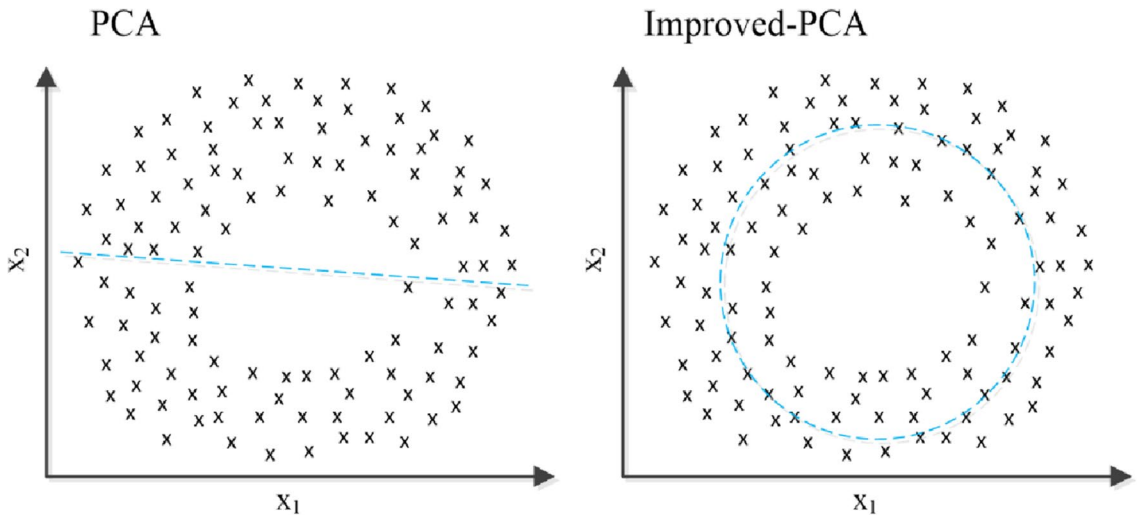

Fig. 6 Comparison of PCA and Improved-PCA

$$V^T\varphi(x') = \left(\frac{1}{\sqrt{\lambda}}X^T u\right)^T \varphi(x') = \frac{1}{\sqrt{\lambda}}u^T X\varphi(x') = \frac{1}{\sqrt{\lambda}}u^T\begin{bmatrix}\varphi(x_1)^T\\ \vdots \\ \varphi(x_N)^T\end{bmatrix}\varphi(x') = \frac{1}{\sqrt{\lambda}}u^T\begin{bmatrix}\kappa(x_1,x')\\ \vdots \\ \kappa(x_N,x')\end{bmatrix}. \quad (16)$$

By applying the kernel function to the low-dimensional space, the calculation can get nearly the same result as in the high-dimensional space, as seen in the projection above. PCA is a linear transformation of the coordinate axes, meaning that the new base remains a straight line following the transformation. However, the kernel-based PCA performs a nonlinear modification of the coordinate axes, and the new basis projected by the data is no longer a straight line but rather a curve or surface (as shown in Fig. 6).

Obviously, the kernel-based method PCA can separate different data classes, while PCA makes a projection of them. This shows the advantages of PCA based on the kernelization method.

3.3 Fast Independent Component Analysis (FICA) Algorithm

Independent Component Analysis (ICA), refers to an analysis process that separates or approximates the source signal when only the mixed signal is known, without knowing the source signal, the noise, and the mixing mechanism. The algorithm considers the observed signal as a linear combination of several statistically independent components, and what ICA has to do is a demixing process.

Suppose that m_t is the EMG signal acquired in the experiment, which actually consists of the source signal n_t from the muscle and the noise v_t from the other sensors during the acquisition. The signal can be approximated as a linear mixed system, expressed by the following equation.

$$m_t = A \times n_t + v_t. \quad (17)$$

The purpose of the ICA algorithm is to separate the source signal n_t from the above equation and, by calculation, obtain a signal y_t that is similar to the original signal.

In recent years, a fast ICA algorithm (FICA) has emerged, which is obtained based on a fixed-point recursive algorithm, and it works for any type of data. It was proposed by Hyvärinen et al., at the University of Helsinki, Finland. After optimizing the cumulative distribution function in the traditional ICA algorithm with the iterative formula, we can obtain the FICA algorithm. FICA uses a fixed-point iterative optimization algorithm, which makes the convergence faster and more robust.

4 Prediction Algorithms

4.1 Feature Extraction Based on Convolutional Neural Networks

Over recent years, numerous fields have implemented deep learning techniques. CNN is a feedforward neural network with convolutional operations and a depth structure commonly employed in image processing and natural language processing. Similar to essential neural networks, convolutional neural networks [10] are biologically inspired by feedforward artificial neural networks. Each hidden CNN layer consists of a convolutional layer and a pooling layer. The last layer of CNN is usually a fully connected layer used for data classification.

Figure 7 shows the overall architecture of the CNN, which consists of three types of layers: convolutional, max-pooling, and classification. Even layers are utilized for convolution, while odd layers are used for maximum pooling. The output nodes of the convolution and max-pooling layers are combined to form the feature map, which is a 2D plane.

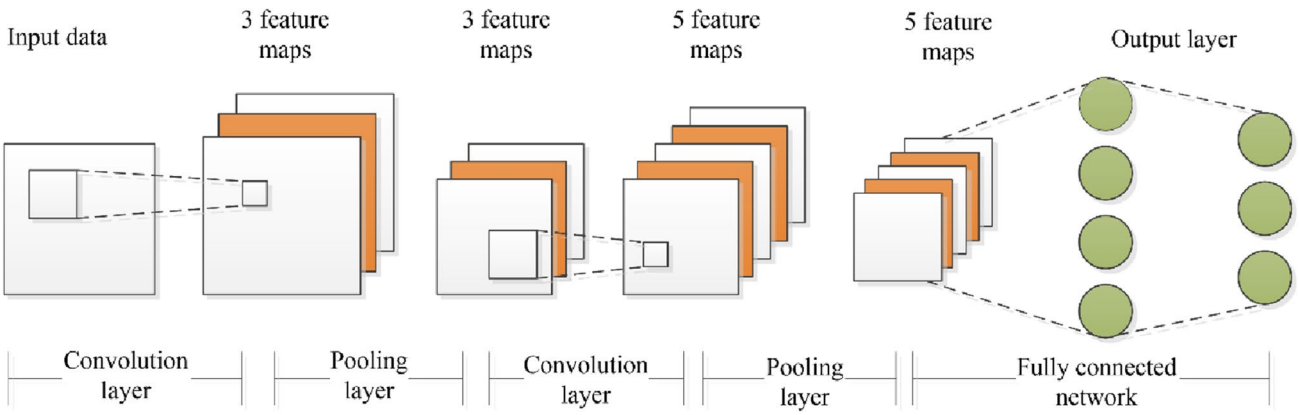

Fig. 7 The overall framework of CNN

4.1.1 Convolutional Layer

Convolutional layers take advantage of three critical ideas that can help improve machine learning systems: sparse interaction, parameter sharing, and covariant representation. The convolutional layer of a convolutional neural network operates by applying convolution to each data set. The two-dimensional discrete convolution operation is shown in Eqs. 18 and 19.

$$S[n_1, n_2] = \sum_{m=1}^{M_1} \sum_{m=1}^{M2} x[m_1, m_2] w[n_1 - m_1, n_2 - m_2]. \tag{18}$$

$$C = \frac{1}{N} \sum_{i=1}^{N} x_t x_i^T. \tag{19}$$

4.1.2 Pooling Layer

Pooling functions replace the output of a layer with the summary statistics of the previous layer's output. This layer in the architecture accelerates the training and categorization. x_n is a vector holding the pooled data of the dataset. The pooling function is represented in the following equation.

$$x_n = \{x_j, ..., x_N\}. \tag{20}$$

$$\hat{x_n} = f(x_n, x_{n+1}, x_{n+2}) = f(x_n). \tag{21}$$

The pooling layer may include the set's greatest value, the average value, the parametric value, and the weighted mean of the pool. The maximum pool is utilized according to Eq. 22.

$$f(x_n) = argmax(x_n). \tag{22}$$

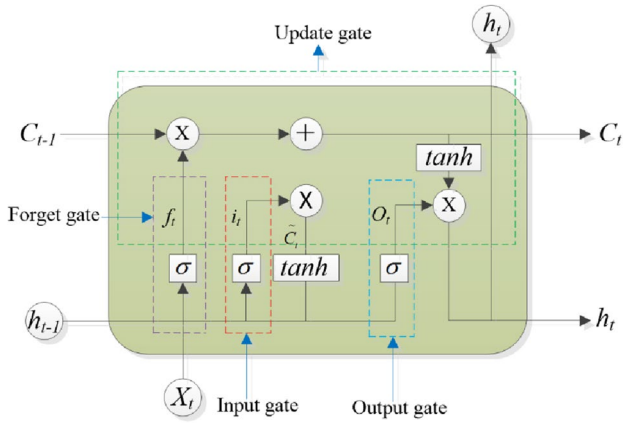

Fig. 8 LSTMcell

4.2 Serial Regression Based on Long Short-Term Memory

In recent years, LSTM has been widely used in speech recognition, sentiment analysis, text analysis and other fields. The LSTM forms the lower layer of the model proposed in this paper. This layer stores the temporal information of the important attributes of the EMG signal. The memory channel and gate mechanism (the forgetting gate, input gate, update gate, and output gate) are shown in Fig. 8.

Cell state (C_{t-1}–C_t) is the foundation of the LSTM design. Cell state holds the hidden state information for the current time. The hidden state information includes both the hidden state from the preceding time step and the temporary hidden state of the current time step. In addition, the LSTM includes a unique "gate" structure for removing or adding information to the cell state.

4.3 Forgotten Gate

The first step in LSTM is to decide the information to be discarded in the cell state. This decision is made via the forgetting gate layer. The forgotten gate reads h_{t-1} and x_t and outputs a number between 0 and 1 for each cell state number. 1 indicates "keep totally," and 0 indicates "discard completely."

$$f_t = \sigma(W_f.[h_{t-1}, x_t] + b_f). \tag{23}$$

4.4 Input Gate

Afterward, the input gate determines which new information may be added to the cell's state. Each tanh-layer generates a vector that can be substituted for the update (Eqs. 24, 25). These two components will be merged to update the cell state.

$$i_t = \sigma(W_i.[h_{t-1}, x_t] + b_i). \tag{24}$$

$$\tilde{C}_t = \tanh(W_c.[h_{t-1}, x_t] + b_c). \tag{25}$$

4.5 Update Gate

The function of the update gate is to transform old cell data (C_{t-1}) into new cell data (C_t). The update gate picks a portion of the old cell information for erasure by the forget gate. Afterward, the input gate selects a portion of the candidate cell information to combine with the new cell information C_t.

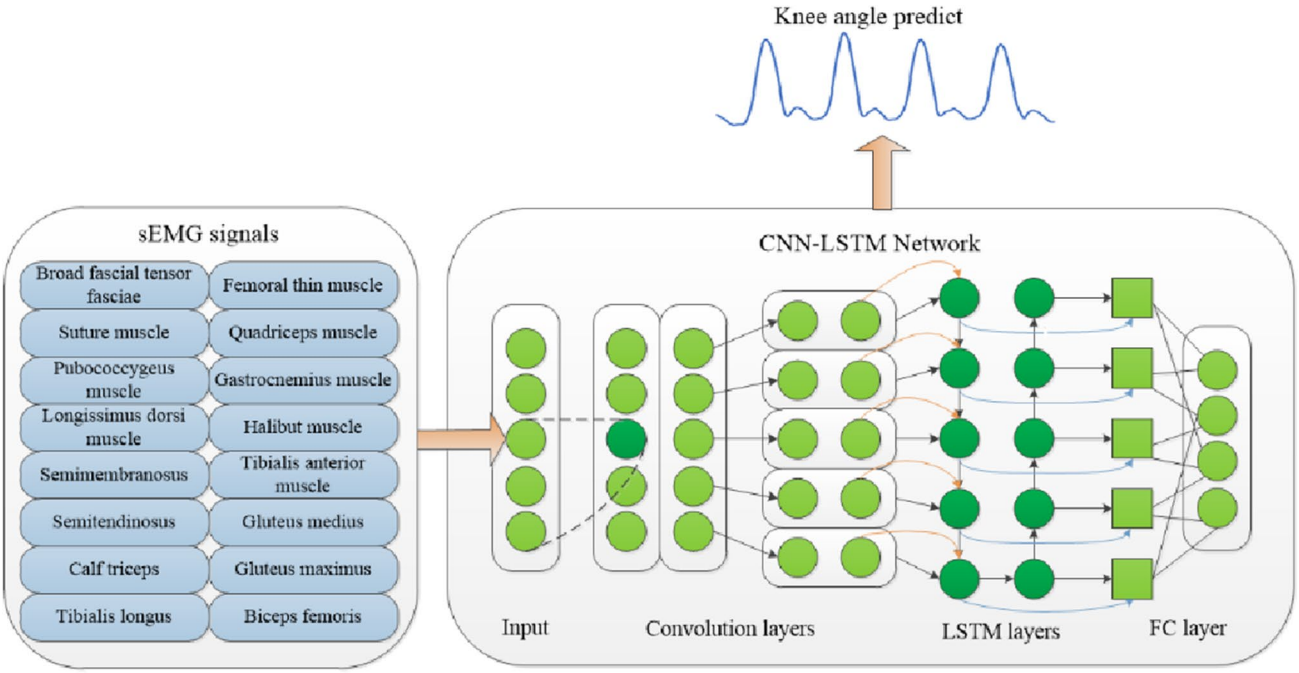

Fig. 9 The structure of CNN-LSTM

$$C_t = f_t * C_{t-1} + i_t * \tilde{C}_t. \tag{26}$$

4.6 Output Gate

After updating the cell's state, it is necessary to determine the output cell's state based on the input values h_{t-1} and x_t. The cell state is transmitted through the tanh-layer to get a vector of values between [− 1, 1], multiplied by the output gate's judgment criteria to produce the cell's output.

$$o_t = \sigma\left(W_o\left[h_{t-1}, x_t\right] + b_o\right), \tag{27}$$

$$h_t = o_t * tanh(C_t), \tag{28}$$

where h_t is the output vector result of the memory cell at time t (as Fig. 8 shows). $W_{f,i,c,o}$ are the weights matrices and $b_{f,i,c,o}$ the bias vectors.

4.7 CNN-LSTM Training Model

In this study, by integrating CNN and LSTM, we propose a new deep learning scheme. The feature sequences from the CNN layer are considered as the input to the LSTM. The CNN-LSTM structure proposed in this paper is shown in Fig. 9. It consists of a CNN layer, an LSTM layer, and a fully connected (FC) layer. The CNN layer is used to receive and process the sEMG signals from 16 different locations of the human lower limbs. On the other hand, the dataset is divided into two parts: 80% for training the model and 20% for validating the results. This network structure consists of an input layer (inputting sensor variables), an output layer (extracting features to the LSTM), and several hidden layers. The hidden layers include the convolutional, ReLU, activation, and pooling layers. The neural network generates a weight for each input to determine a specific output based on this structure. The CNN structure consists mostly of five convolutional layers and five pooling layers in the hybrid model. Respectively, the activation function has 64, 128, 256, 128, and 64 convolutional kernels. The LSTM model contains five hidden layers with 64, 128, 256, 128, and 64 neurons, respectively. The underlying layers of the model are two fully connected layers, which have 4096 and 2048 neurons, respectively.

Sensitive deep learning parameters are considered to maximize accuracy and optimize training time. The model is trained with 150 data points per batch, 120 epochs maximum, and 15 iterations per epoch. After all architectures have been trained, the confusion matrix is used to evaluate

the network's performance. This allows for the calculation of accuracy and recalls for each category.

4.8 Experimental Evaluation

To evaluate the model, a set of evaluation measures were chosen. According to [36], the root means square error (RMSE) and the Pearson correlation coefficient were selected to assess the accuracy of the predictions. A parameter's mean squared error (MSE) is the expected value of the squared difference between its estimated and actual value. The root means squared error (RMSE) equals the square root of the squared mean error (MSE). These metrics are defined in the following manner:

$$MSE = \frac{1}{n}\sum_{i=1}^{n}(Y_t - \hat{Y}_p)^2, \tag{29}$$

$$RMSE = \sqrt{\frac{1}{n}\sum_{i=1}^{n}(Y_t - \hat{Y}_p)^2}. \tag{30}$$

Pearson correlation, also known as cumulative correlation, is a method invented by the British statistician Pearson in the twentieth century to determine linear correlation. The Pearson correlation coefficient is frequently used to analyze data that conforming a linear relationship or a normal distribution. It can be calculated as Eq. 31.

$$\rho_{Y_t,Y_p} = \frac{\sum(Y_t - \overline{Y_t})(Y_p - \overline{Y_p})}{\sqrt{\sum(Y_t - \overline{Y_t})^2(Y_p - \overline{Y_p})^2}}, \tag{31}$$

where: Y_t is the real Knee angle value, $\hat{Y}_p$ is the predicted value, and n is the number of Y_t.

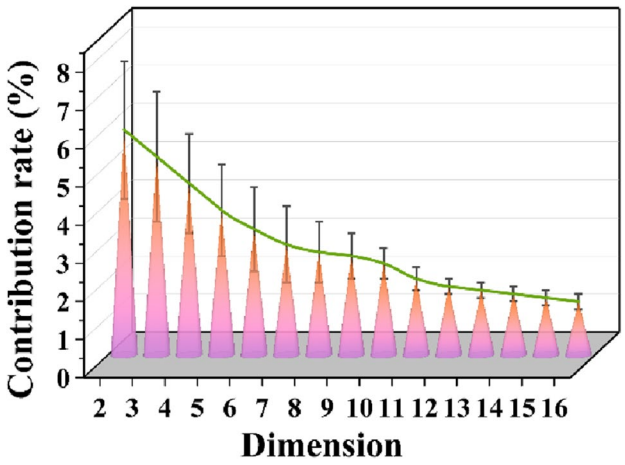

Fig. 11 Difference of principal component contributions under the same dimension

5 Experimental Results and Analysis

This chapter composed a new dataset including 16 different EMG signals and corresponding knee angles. Corresponding data were collected from 10 different individuals (five males, five females). The replicated data were then preprocessed in various methods (FICA/PCA/Improved PCA, respectively). Immediately after, these data were imported into the previously built models (CNN-LSTM) separately for data prediction. Each set of data was repeatedly trained and predicted 200 times. The model automatically recorded the training error for each training. Finally, the effects of various data processing methods on prediction accuracy and time spent are compared. In addition, the model training time and Pearson correlation coefficients are compared for different scenarios. To reflect the superiority of the prediction models proposed in this paper, other prediction models are used for

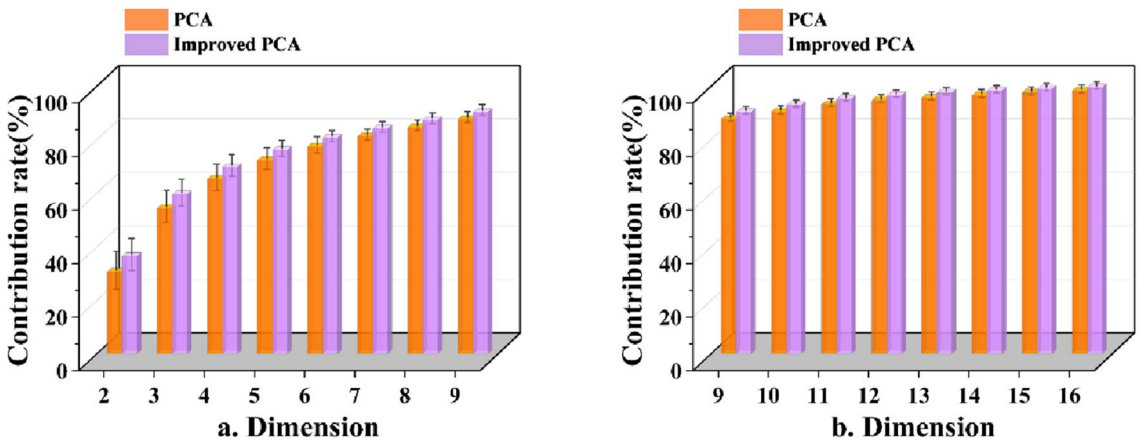

Fig. 10 Contribution of principal components under different dimensions

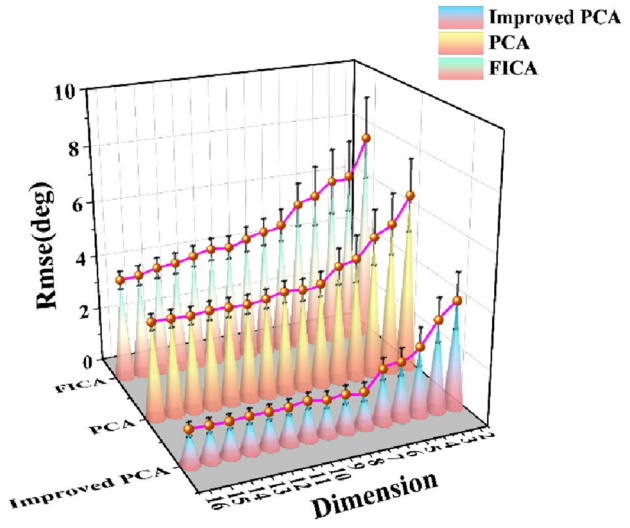

Fig. 12 Comparison of prediction errors in different dimensions

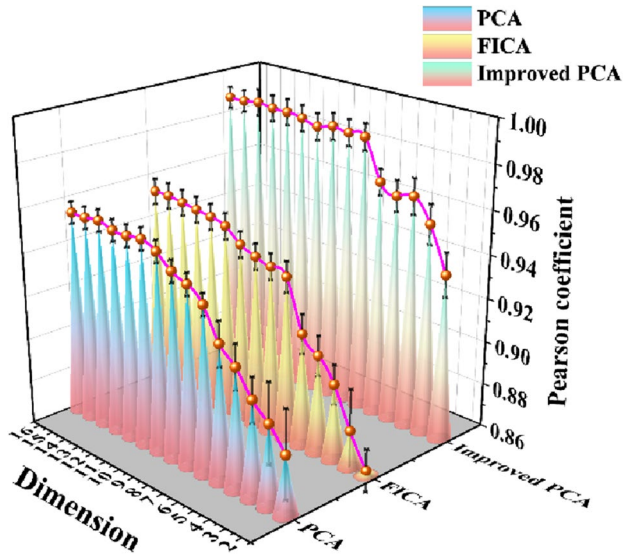

Fig. 13 Comparison of Pearson's correlation coefficients under different dimensions

comparison. The study's findings are presented as the mean plus standard deviation to highlight the algorithms' consistent performance.

5.1 Analysis 1: Principal Component Contribution Rates Under Different Dimensions

To select the best data input dimensions, we downscaled the sEMG signals of these 16 different channels. All dimensions were tried, and their principal component contribution rates were recorded. Figure 10 shows the difference in principal component contribution rates between the improved PCA algorithm and the traditional PCA algorithm for the same dimensions. As shown in Fig. 11, the principal component contribution rate gradually increases from low to high dimensions. Apparently, the increasing trend of the principal component contribution is significantly greater among the 2–8 dimensions than among the 9–16 dimensions. As dimensions rise, the increase of primary component contribution tends to level off. Regarding principle component extraction rate, the improved PCA algorithm is much superior to the standard PCA method (most evident in dimensions 2–8).

The improved PCA approach presented in this study performs a nonlinear mapping of the sEMG signal using a Gaussian kernel function for nonlinear dimensionality reduction. Then, the centralization process was performed. Unlike the conventional PCA method, the resulting feature vectors are not the projected axes but the projected coordinates. For linearly indistinguishable datasets, the improved PCA method maps them to higher dimensions and divides them. The results demonstrate that this method can more efficiently extract the principal components of sEMG signals in a nonlinear state.

5.2 Analysis 2: Comparison of Prediction Accuracy Under Different Dimensions

Then, the downscaled data were classified and imported into the CNN-LSTM model for prediction. Finally, the prediction errors for 10 different experimental subjects and the Pearson correlation coefficients were obtained. Immediately after, the predicted data are collated and compared. Figure 12 shows that the prediction accuracy gradually improves as the dimensionality increases (either in FICA/PCA/Improved PCA). Obviously, the improved PCA method always has the smallest prediction error, followed closely by the PCA method and finally the FICA method.

Figure 13 compares the Pearson correlation coefficients in different dimensions. It can be found that as the dimensionality increases, the Pearson correlation coefficient also increases. Obviously, the improved PCA algorithm achieved the highest Pearson correlation coefficient. In practical applications of sEMG in the field of assisted exoskeletons, errors higher than 5 degrees are unacceptable for achieving soft control. Excessive prediction errors may lead to ineffective control and interfere with the task process. From this perspective, the processing data of the improved PCA shows the most stable performance (among the various algorithms).

5.3 Analysis 3: Comparison of Prediction Accuracy Under Different Data Processing Methods

Figure 14 visually compares the prediction results of the data under each different pre-processing method. The data

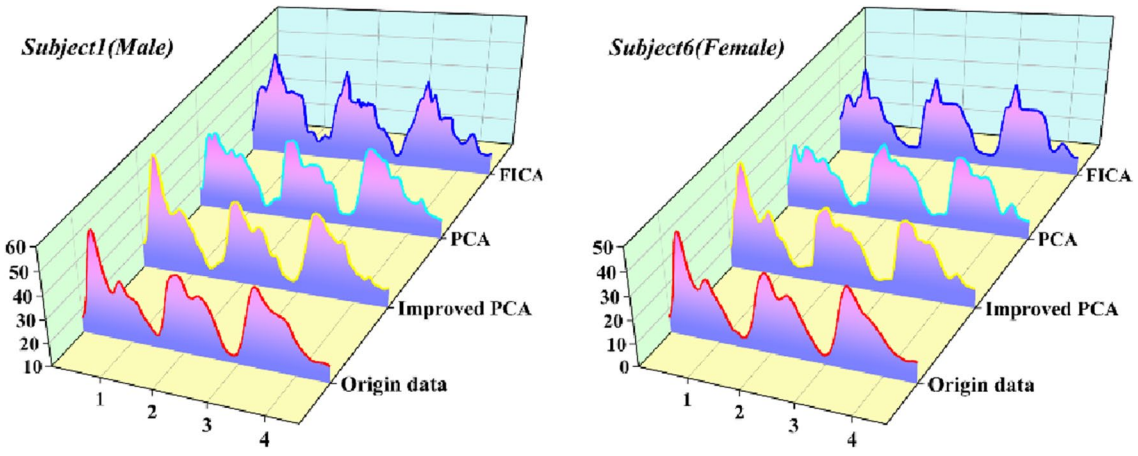

Fig. 14 Prediction results under different methods

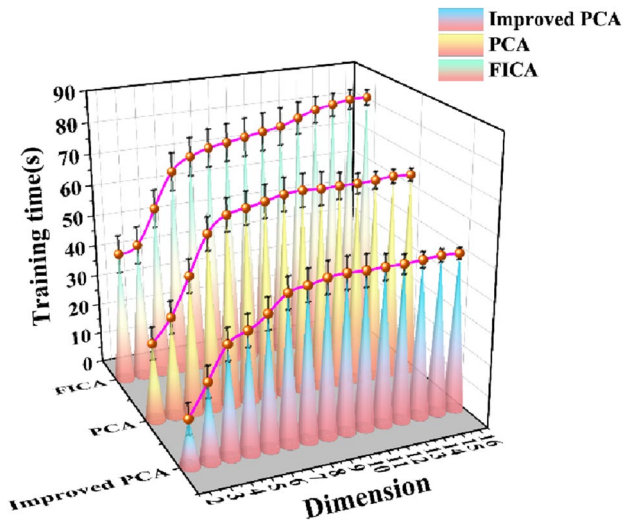

Fig. 15 Comparison of training time under different dimensions

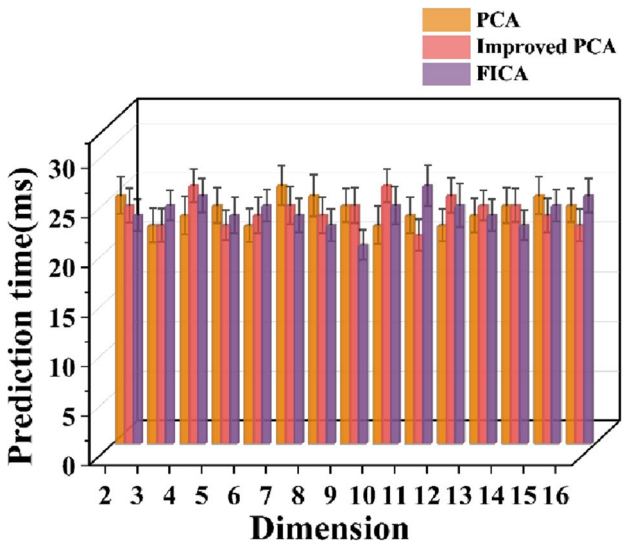

Fig. 16 Comparison of prediction times under different dimensions

from two volunteers (one male, one female) are used for comparison. Since the step size of males is relatively larger than that of females. The knee angles collected in the experiment for females were smaller than those for males. It can be seen from the figure that the prediction results of the data processed by the improved PCA algorithm are closest to the experimentally collected data. Then comes the data processed by the PCA algorithm, and finally, the data processed by FICA.

5.4 Analysis 4: Comparison of Training and Prediction Time Under Different Dimensions

Next, the algorithm prediction elapsed time (both training and prediction time) was compared under different dimensions. All data were processed by Python on a personal server (with 3.30 GHz Intel Xeon CPU and GUP-NVIDIA 2080Ti). Figure 15 illustrates each method instance's average training and test run times. It is evident that as the dimension rises, the training time of the algorithm gradually increases. Similar to the prior contribution of the primary component, the range of increase in training time is more extensive bigger for dimensions 2–8 than dimensions 9–16. Notably, once the algorithm training phase is complete, the prediction times are practically identical (in a concise time, as shown in Fig. 16). Such restrictions are tolerable for the majority of communication systems. With the rapid advancement of graphics processing unit (GPU) technology, it is anticipated that the method will become even more effective.

Table 2 Average accuracy of the model for 20 runs

Algorithm	Pearson coefficient	RMSE(deg)	Training time(s)	Forecast time(ms)
RF(FICA)	0.889	6.13 ± 1.62	5.05 ± 0.98	16.8 ± 1.1
RF(PCA)	0.895	5.71 ± 1.21	5.21 ± 0.94	17.4 ± 1.4
RF(Improved PCA)	0.932	4.81 ± 1.54	5.04 ± 1.03	17.8 ± 1.2
SVR(FICA)	0.869	4.71 ± 1.21	79.87 ± 5.71	35.5 ± 3.2
SVR(PCA)	0.875	4.52 ± 1.26	85.52 ± 5.68	34.4 ± 2.7
SVR(Improved PCA)	0.886	4.11 ± 1.06	74.97 ± 5.14	36.2 ± 2.9
BP(FICA)	0.919	3.89 ± 1.62	125.41 ± 13.25	33.3 ± 2.7
BP(PCA)	0.923	3.75 ± 1.57	127.51 ± 14.84	32.1 ± 2.5
BP(Improved PCA)	0.947	1.78 ± 0.42	114.92 ± 12.72	33.8 ± 2.4
CNN-LSTM (FICA)	0.951	3.97 ± 0.64	54.54 ± 2.12	25.5 ± 1.4
CNN-LSTM(PCA)	0.965	3.72 ± 0.36	58.24 ± 2.41	26.5 ± 1.5
CNN-LSTM(Improved PCA)	0.985	1.34 ± 0.25	46.55 ± 1.85	25.4 ± 1.2

5.5 Analysis 5: Comparsion with Other Models

In the end, the performance of the CNN-LSTM model is compared with other algorithms in terms of prediction results. All data were processed by Python on a personal server (with 3.30 GHz Intel Xeon CPU and GUP-NVIDIA 2080Ti). Table 2 shows the comparison results. It can be easily found that the CNN-LSTM model combined with the improved PCA algorithm has the best performance (both in terms of prediction/training time and prediction accuracy). Moreover, the traditional PCA still has an advantage over the prediction results of the data after the original data filtering process.

6 Discussion

By comparing the prediction accuracy, computational time consumption, and correlation coefficients under different combinations of algorithms, a new method (CNN-LSTM + Improved PCA) for predicting knee angles using EMG signals is proposed in this paper. With the EMG signals collected from the training experiments, the model can efficiently predict the corresponding knee angles from the input sEMG signals. The prediction accuracy under different conditions was analyzed and compared. It can be said that the new method proposed in this paper outperforms other machine learning-based methods in terms of performance. The proposed method (CNN-LSTM combined with improved PCA) in this paper yields an accuracy of about 98.5%. With the above discussion, the excellent performance of the proposed method can be attributed to two reasons. One is the combination of CNN and LSTM, which can extract more practical features. The other one is the special interaction mechanism that can increase the diversity of features. Comparing the model parameters (Pearson correlation coefficient, RMSE, training time, and prediction time) under the same data, it is possible to determine that the new method (CNN + LSTM) described in this study has more advantages than existing machine learning methods. This permits the creation of auxiliary devices with high precision. This study aims to assess the impact of signal pre-processing techniques on the accuracy of prediction. Additionally, this article explores the relationship between the sEMG signal and the human joint angle to design a high-precision EMG controller for exoskeletons in future research. It facilitates the use of the sEMG signal to control the exoskeleton and provides intelligent support.

7 Conclusion

This work aims to investigate the effect of pre-processing sEMG signals on the prediction results and lay the foundation for constructing an accurate and responsive exoskeleton robot controller. A new method based on CNN-LSTM with an improved PCA algorithm structure is proposed in this paper to predict the knee joint angle. Experimental data from 10 individuals were collected to demonstrate the method's superiority. As a result, the improved PCA method can extract the principal components from the data more efficiently and help the model achieve faster convergence than the traditional PCA method. Comparing the prediction results in various cases shows that improved PCA and CNN-LSTM produce the best results while maintaining computational efficiency. The experimental results also show that the combination of CNN and LSTM possesses the best prediction results compared to other existing models. The anticipated work will continue to expand in the future. To develop more flexible and efficient exoskeleton devices, the study of ankle joint angle and hip joint angle during the task

is equally important. In addition, multi-source signal fusion of force signals, motion signals (IMU) and sEMG signals to predict human motion is another area that should be investigated in the future. Moreover, due to the complexity of human musculoskeletal models, selecting the optimal location for signal acquisition is a topic of research and interest.

Acknowledgements Thanks to the experiment participants and Nanjing University of Science and Technology for their support of this study.

Author Contributions Conceptualization: MZ and XRG; methodology: MZ, XRG, and ZL; software: MZ and XRG; validation: ZL; formal analysis: MZ; investigation: MZ; resources: ZW; data curation: MZ; writing—original draft: MZ; visualization: MZ; supervision: KSC.

Funding The authors did not receive support from any organization for the submitted work.

Data Availability The datasets used or analysed during the current study are available from the corresponding author on reasonable request.

Code Availability The code used during the current study are available from the corresponding author on reasonable request.

Declarations

Conflict of Interest The authors declare that they have no known competing financial interests or personal relationships that could have appeared to influence the work reported in this paper.

Ethical Approval The experiment was approved by the review board of The First Affiliated Hospital of Nanjing Medical University and was conducted in accordance with the Declaration of Helsinki.

Consent to Participate This study was approved by the ethical committee of The First Affiliated Hospital of Nanjing Medical University, and all participants provided informed verbal consent. We obtained the verbal consent of the patient or his immediate family members by telephone and the ethics committee approved this procedure.

Consent for Publication Written informed consent for publication was obtained from all participants.

References

1. Wang, Z. B., Wang, Z. B., Yang, Y. H., Wang, C. Z., Yang, G., & Li, Y. F. (2022). Mechanical design and research of wearable exoskeleton assisted robot for upper limb rehabilitation. *Chinese Journal of Medical Instrumentation, 46*, 42–46. https://doi.org/10.3969/j.issn.1671-7104.2022.01.009 in Chinese.
2. Amilibia, M. Z., Cortes, C., Simonetti, A. B., Satrustegi, A., Iturburu, M., Reina, I., Finez, J., Alonso-Arce, M., & Callejo, P. (2021). Preliminary evaluation of an objective assessment approach from session data in exoskeleton-assisted gait rehabilitation after SCI. *In 43rd Annual International Conference of the IEEE Engineering in Medicine and Biology Society Mexico, San Luis Potosi.* https://doi.org/10.1109/EMBC46164.2021.9630352
3. Inoue, J., Kimura, R., Shimada, Y., Saito, K., Kudo, D., Hatakeyama, K., Watanabe, M., Maeda, K., Iwami, T., Matsunaga, T., & Miyakoshi, N. (2022). Development of a Gait rehabilitation robot using an exoskeleton and functional electrical stimulation: validation in a pseudo-paraplegic model. *Progress in Rehabilitation Medicine, 7*, 20220001. https://doi.org/10.2490/prm.20220001
4. Liu, C., Liang, H. B., Ueda, N., Li, P., Fujimoto, Y., & Zhu, C. (2020). Functional evaluation of a force sensor-controlled upper-limb power-assisted exoskeleton with high back drivability. *Sensors, 20*, 6379. https://doi.org/10.3390/s20216379
5. Harith, H. H., Mohd, M. F., & Sowat, S. N. (2021). A preliminary investigation on upper limb exoskeleton assistance for simulated agricultural tasks. *Applied Ergonomics, 95*, 103455. https://doi.org/10.1016/j.apergo.2021.103455
6. Pinho, J. P., & Forner-Cordero, A. (2022). Shoulder muscle activity and perceived comfort of industry workers using a commercial upper limb exoskeleton for simulated tasks. *Applied Ergonomics, 101*, 103718. https://doi.org/10.1016/j.apergo.2022.103718
7. Huang, R., Wu, Q., Qiu, J., Cheng, H., Chen, Q., & Peng, Z. N. (2020). Adaptive gait planning with dynamic movement primitives for walking assistance lower exoskeleton in uphill slopes. *Sensors and Materials, 32*, 1279–1291. https://doi.org/10.18494/SAM.2020.2550
8. Seo, K., Lee, J., & Park, Y. J. (2017). Autonomous hip exoskeleton saves metabolic cost of walking uphill. *In: IEEE 2017 International Conference on Rehabilitation Robotics. London, United Kingdom*. https://doi.org/10.1109/ICORR.2017.8009254
9. Liu, H., Tao, J., Lyu, P., & Tian, F. (2019). Human-robot cooperative control based on sEMG for the upper limb exoskeleton robot. *Robotics and Autonomous Systems, 125*, 103350. https://doi.org/10.1016/j.robot.2019.103350
10. Vijayvargiya, A., Khimraj Kumar, R., & Dey, N. (2021). Voting-based 1d cnn model for human lower limb activity recognition using semg signal. *Physical and Engineering Sciences in Medicine, 44*, 1297–1309. https://doi.org/10.1007/s13246-021-01071-6
11. Gao, B. F., Wei, C., Ma, H. D., Yang, S., Ma, X., & Zhang, S. Y. (2018). Real-time evaluation of the signal processing of semg used in limb exoskeleton rehabilitation system. *Applied Bionics and Biomechanics, 2018*, 1–6. https://doi.org/10.1155/2018/1391032
12. Cheng, J., Chen, X., & Shen, M. F. (2013). A framework for daily activity monitoring and fall detection based on surface electromyography and accelerometer signals. *IEEE Journal of Biomedical and Health Informatics, 17*, 38–45. https://doi.org/10.1109/TITB.2012.2226905
13. Farina, D., & Negro, F. (2012). Accessing the neural drive to muscle and translation to neurorehabilitation technologies. *IEEE Reviews in Biomedical Engineering, 5*, 3–14. https://doi.org/10.1109/RBME.2012.2183586
14. Nurhazimah, N., Mohd, A. A. R., Shin-Ichiroh, Y., Siti, A., Hairi, Z., & Saiful, A. M. (2016). A Review of classification techniques of EMG signals during isotonic and isometric contractions. *Sensors, 16*, 1304. https://doi.org/10.3390/s16081304
15. Johan, N., Axel, S., Edmar, C., Daryl, C., Edward, R., Alvaro, F., Johrdan, H., Briggitte, S., & Leonardo, M. C. (2020). Preliminary design of an Intention-based sEMG-controlled 3 DOF upper limb exoskeleton for assisted therapy in activities of daily life in patients with hemiparesis. *In: 2020 8th IEEE RAS/EMBS International Conference for Biomedical Robotics and Biomechatronics. New York, USA*. https://doi.org/10.1109/BioRob49111.2020.9224397
16. Wang, C., Guo, Z. M., Duan, S. C., He, B. L., Yuan, Y., & Wu, X. Y. (2021). A real-time stability control method through sEMG interface for lower extremity rehabilitation exoskeletons. *Frontiers in Neuroscience, 15*, 645374. https://doi.org/10.3389/fnins.2021.645374
17. Vijayvargiya, A., Singh, P. L., Verma, S. M., Kumar, R., & Bansal, S. (2019). Performance comparison analysis of different classifier

for early detection of knee osteoarthritis. *Sensors for Health Monitoring, 5*, 243–257. https://doi.org/10.1016/B978-0-12-819361-7.00012-9

18. Fang, H. G., Wang, J., & Kankaanpaa, M. (2005). Comparison of lumbar muscle sEMG between health and LBP patients during dynamic back extensions. *In: 2005 IEEE Engineering in Medicine and Biology 27th Annual Conference. Shanghai, China*. https://doi.org/10.1109/IEMBS.2005.1616232
19. Chen, Y. M., Yang, Z. L., & Wen, Y. L. (2021). A Soft exoskeleton glove for hand bilateral training via surface EMG. *Sensors, 21*, 578. https://doi.org/10.3390/s21020578
20. Cisnal, A., Pérez-Turiel, J., Fraile, J. C., Sierra, D., & Fuente, E. D. L. (2021). RobHand: a hand exoskeleton with real-time EMG-driven embedded control. Quantifying hand gesture recognition delays for bilateral rehabilitation. *IEEE Access, 9*, 137809–137823. https://doi.org/10.1109/ACCESS.2021.3118281
21. Zhuang, Y., Leng, Y., Zhou, J., Song, R., Li, L., & Su, S. W. (2020). Voluntary control of an ankle joint exoskeleton by able-bodied individuals and stroke survivors using emg-based admittance control scheme. *IEEE Transactions on Biomedical Engineering, 68*, 695–705. https://doi.org/10.1109/TBME.2020.3012296
22. Lyu, M. X., Chen, W. H., Ding, X. L., Wang, J. H., Pei, Z. C., & Zhang, B. C. (2019). Development of an EMG-controlled knee exoskeleton to assist home rehabilitation in a game context. *Frontiers in Neurorobotics*. https://doi.org/10.3389/fnbot.2019.00067
23. Hajian, G., Morin, E., & Etemad, A. (2019). PCA-based channel selection in high-density EMG for improving force estimation. *In: 2019 41st Annual International Conference of the IEEE Engineering in Medicine and Biology Society. Berlin, Germany*. https://doi.org/10.1109/EMBC.2019.8857118
24. Wang, G., Zhang, Y. Y., & Wang, J. (2014). The analysis of surface EMG signals with the wavelet-based correlation dimension method. *Computational and Mathematical Methods in Medicine, 2014*, 284308. https://doi.org/10.1155/2014/284308
25. Sapsanis, C., Georgoulas, G., Tzes, A., & Lymberopoulos, D. (2013). Improving EMG based classification of basic hand movements using EMD. *In: 2013 35th Annual International Conference of the IEEE Engineering in Medicine and Biology Society. Osaka, Japan*. https://doi.org/10.1109/EMBC.2013.6610858
26. Dhar, P., Garg, V. K., & Rahman, M. A. (2022). Enhanced feature extraction-based CNN approach for epileptic seizure detection from EEG signals. *Journal of Healthcare Engineering, 2022*, 3491828. https://doi.org/10.1155/2022/3491828
27. Wu, J. H., Zhao, T., Zhang, Y. K., Xie, L., Yan, Y., & Yin, E. W. (2021). Parallel-inception CNN approach for facial sEMG based silent speech recognition. *In: 2021 43rd Annual International Conference of the IEEE Engineering in Medicine & Biology Society. Mexico, San Luis Potosi*. https://doi.org/10.1109/EMBC46164.2021.9630373
28. Da, U. J., & Lim, K. M. (2021). Combined deep CNN-LSTM network-based multitasking learning architecture for noninvasive continuous blood pressure estimation using difference in ECG-PPG features. *Scientific Reports, 11*, 13539. https://doi.org/10.1038/s41598-021-92997-0
29. Zhang, B., Zhang, H. W., Zhao, G. M., & Lian, J. (2020). Constructing a PM25 concentration prediction model by combining auto-encoder with Bi-LSTM neural networks. *Environmental Modelling & Software, 124*, 104600.
30. Konrad, P. (2005). *The ABC of EMG: A practical introduction to kinesiological electromyography*. USA, Noraxon: Scottsdale, AZ. http://www.demotu.org/aulas/ABCofEMG.pdf. Accessed 29 July 2009.
31. Leardini, A., Sawacha, Z., Paolini, G., Ingrosso, S., Nativo, R., & Benedetti, M. G. (2007). A new anatomically based protocol for gait analysis in children. *Gait & Posture, 26*, 560–571. https://doi.org/10.1016/j.gaitpost.2006.12.018
32. Chowdhury, R. H., Reaz, M. B. L., Ali, M., Bakar, A., Chellappan, K., & Chang, T. (2013). Surface electromyography signal processing and classification techniques. *Sensors, 13*, 12431–12466. https://doi.org/10.3390/s130912431
33. Dong, S. X., Zhou, Y., Chen, T. Y., Li, S., Gao, Q. T., & Ran, B. (2021). An integrated empirical mode decomposition and Butterworth filter based vehicle trajectory reconstruction method. *Physica A: Statistical Mechanics and its Applications, 583*, 126295. https://doi.org/10.1016/j.physa.2021.126295
34. Huang, S. G., Chung, M. K., & Qiu, A. (2021). Fast mesh data augmentation via Chebyshev polynomial of spectral filtering. *Neural Networks, 143*, 198–208. https://doi.org/10.1016/j.neunet.2021.05.025
35. Ni, A., & Qin, L. X. (2021). Performance evaluation of transcriptomics data normalization for survival risk prediction. *Briefings in Bioinformatics, 22*, 257. https://doi.org/10.1093/bib/bbab257
36. Tang, Z. C., Zhang, K. J., Sun, S. Q., Gao, Z. G., Zhang, L. K., & Yang, Z. L. (2014). An upper-limb power-assist exoskeleton using proportional myoelectric control. *Sensors, 14*, 6677–6694. https://doi.org/10.3390/s140406677